HAL
open science

Examination of Water Quantification and Incorporation in Transition Zone Minerals: Wadsleyite, Ringwoodite and Phase D Using ERDA (Elastic Recoil Detection Analysis)

Nathalie Bolfan-Casanova, Federica Schiavi, Davide Novella, Hélène Bureau, Caroline Raepsaet, Hicham Khodja, Sylvie Demouchy

To cite this version:

Nathalie Bolfan-Casanova, Federica Schiavi, Davide Novella, Hélène Bureau, Caroline Raepsaet, et al.. Examination of Water Quantification and Incorporation in Transition Zone Minerals: Wadsleyite, Ringwoodite and Phase D Using ERDA (Elastic Recoil Detection Analysis). Frontiers in Earth Science, 2018, 6, pp.75. 10.3389/feart.2018.00075 . cea-01818386

HAL Id: cea-01818386

https://cea.hal.science/cea-01818386v1

Submitted on 19 Jun 2018

HAL is a multi-disciplinary open access archive for the deposit and dissemination of scientific research documents, whether they are published or not. The documents may come from teaching and research institutions in France or abroad, or from public or private research centers.

L'archive ouverte pluridisciplinaire **HAL**, est destinée au dépôt et à la diffusion de documents scientifiques de niveau recherche, publiés ou non, émanant des établissements d'enseignement et de recherche français ou étrangers, des laboratoires publics ou privés.

frontiers in Earth Science

ORIGINAL RESEARCH
published: 19 June 2018
doi: 10.3389/feart.2018.00075

Examination of Water Quantification and Incorporation in Transition Zone Minerals: Wadsleyite, Ringwoodite and Phase D Using ERDA (Elastic Recoil Detection Analysis)

Nathalie Bolfan-Casanova[1], Federica Schiavi[1], Davide Novella[1†], Hélène Bureau[2], Caroline Raepsaet[3], Hicham Khodja[3] and Sylvie Demouchy[4]*

[1] Laboratoire Magmas et Volcans, Centre National de la Recherche Scientifique, IRD, OPGC, Université Clermont Auvergne, Clermont-Ferrand, France, [2] Institut de Minéralogie de Physique de la Matière et de Cosmochimie, Centre National de la Recherche Scientifique, UMR 9956 UPMC, MNHN, Sorbonne Université, Paris, France, [3] LEEL, NIMBE, CEA, Centre National de la Recherche Scientifique, CEA Saclay, Université Paris-Saclay, Gif sur Yvette, France, [4] Géosciences Montpellier, Centre National de la Recherche Scientifique, Université Montpellier, Montpellier, France

OPEN ACCESS

Edited by:
Jean-Philippe Perrillat, Claude Bernard University Lyon 1, France

Reviewed by:
Geoffrey David Bromiley, University of Edinburgh, United Kingdom
Sujoy Ghosh, Indian Institute of Technology Kharagpur, India

***Correspondence:**
Nathalie Bolfan-Casanova
n.bolfan@opgc.univ-bpclermont.fr

†Present Address:
Davide Novella, Department of Earth Sciences, University of Cambridge, Cambridge, United Kingdom

Specialty section:
This article was submitted to Earth and Planetary Materials, a section of the journal Frontiers in Earth Science

Received: 19 February 2018
Accepted: 25 May 2018
Published: 19 June 2018

Citation:
Bolfan-Casanova N, Schiavi F, Novella D, Bureau H, Raepsaet C, Khodja H and Demouchy S (2018) Examination of Water Quantification and Incorporation in Transition Zone Minerals: Wadsleyite, Ringwoodite and Phase D Using ERDA (Elastic Recoil Detection Analysis). Front. Earth Sci. 6:75. doi: 10.3389/feart.2018.00075

Hydrous wadsleyite, ringwoodite, and phase D have been synthesized in the MgO-SiO_2-H_2O and MgO-FeO-SiO_2-H_2O systems at mantle transition zone conditions (15–21 GPa and 1,100–1,700°C) to investigate their water incorporation using Elastic Recoil Detection Analysis (ERDA), which is an absolute quantitative method. Wadsleyite and ringwoodite water contents vary from 0.1 to 3.2 wt% H_2O and for ringwoodite containing up to 1.16 wt% H_2O we observe that the (Mg+Fe)/Si ratio vs. water content follows the same trend as for wadsleyite, indicating that H is substituting for Mg as for wadsleyite. We also measured, for the first time, the water content of phase D and observed that it varies from 6.7 to 11.2 wt% H_2O, up to twice less than estimated from electron microprobe analysis totals. Using these experiments, we were able to determine the absorptivity coefficient for OH infrared absorption bands in four wadsleyite and five ringwoodite samples. The average for the two iron-free wadsleyite samples leads to an absorptivity of 69,000 ± 7,000 L/moles H_2O/cm^2, in very good agreement with previous determinations. The wadsleyite with 8 mole% Fe displays an absorptivity of 67,000 ± 5,000 L/moles H_2O/cm^2. The absorptivity values vary from 118,500 ± 5,000 for Fe-free ringwoodite to ±135,000 ± 9,000 for Fe-bearing ringwoodite (10% mole Fe). Our results show that absorptivity coefficient for OH infrared absorption of ringwoodite do not drastically change with Fe content and that the frequency-based calibration of Paterson (1982) under-estimates its water determinations by 50%. This is very important to know when comparing data from different studies where different extinction coefficients have been used.

Keywords: wadsleyite, ringwoodite, water incorporation, tarnsition zone, deep water cycle

INTRODUCTION

The transition zone of the Earth's mantle, located between 410 and 660 km of depth, is composed for more than 60% of the high-pressure polymorphs of olivine, $(Mg, Fe)_2SiO_4$, namely wadsleyite and ringwoodite. Given the high ability of these minerals to incorporate water, as hydrogenated point defects (Inoue, 1994; Smyth, 1994; Bolfan-Casanova et al., 2000), the transition zone is potentially a major reservoir for water within Earth. The recent discovery of the first terrestrial ringwoodite containing 1.5–2 wt% H_2O corroborates the idea that such high water contents in transition zone minerals is not only a laboratory case but a plausible scenario in nature (Pearson et al., 2014). Recently, the importance of phase D has grown as this phase is a potential candidate to transport water in subduction slabs to great depths (Shieh et al., 1998; Ghosh and Schmidt, 2014; Pamato et al., 2015; Walter et al., 2015). Also, extended solid solution with Al has also been reported for this phase, which greatly enhances its thermal stability field, with an aluminum-rich end-member [i.e., $Al_2SiO_4(OH)_2$] being experimentally observed (Pamato et al., 2015).

Many studies have focused on the determination of physical properties of hydrous wadsleyite and ringwoodite such as elasticity (Chang et al., 2015, and references therein), seismic velocities (Inoue et al., 1998) and electrical conductivity (Huang et al., 2005; Yoshino and Katsura, 2012). Knowledge of the effect of water content on these physical properties is essential for interpreting the geophysical characteristics of the transition zone in terms of its water content. It is therefore essential to develop a reliable method to precisely quantify OH concentrations in high pressure minerals.

Until recently Fourier Transform infrared Spectroscopy (FTIR) was the only spectroscopic technique available to assess the water contents in nominally anhydrous minerals (NAMS) (Libowitzky and Rossman, 1996; Demouchy and Bolfan-Casanova, 2016). Indeed, FTIR is a very sensitive technique that also provides information on the speciation of water (i.e., structurally bound water or water in grain boundaries or melt inclusions). However, there are limitations of this technique when working on polymineralic and small-grain sized experimental samples ($<50\,\mu m$) such as peridotite equilibrated at high-pressures, since quantitative FTIR is essentially used in absorbance mode. Another limitation is that the absorptivity of the bands must be known to convert absorbance into concentration. Such calibrations of the absorptivity of OH bands have been carried out previously for several mantle minerals (Bell et al., 1995 for pyroxenes and garnet; Withers et al., 2012 for olivine; Deon et al., 2010 for wadsleyite; Thomas et al., 2015 for ringwoodite). Alternatively, the universal frequency-based calibration of Paterson (1982) or Libowitzky and Rossman (1997) is used. Other methods of quantification need also to be calibrated (e.g., secondary ion mass spectrometry) and unfortunately there are only few methods that are absolute and easily accessible. A further disadvantage of FTIR for transition zone phases is that the infrared radiation is often completely absorbed by very hydrous samples, requiring the use of very thin samples ($<30\,\mu m$) to levels close to the limits of failure.

In this study, we synthesized wadsleyite and ringwoodite with different H contents to carefully investigate the H incorporation in these minerals. In the following, we discuss (1) new water content characterization of wadsleyite and ringwoodite crystals determined by FTIR and ERDA; (2) the determination of new absorptivity coefficients of OH in wadsleyite and ringwoodite to compare to those previously published; (3) the incorporation mechanisms that we observe for wadsleyite and ringwoodite compared to previous reports and (4) finally, we present the first quantitative measurements of the water concentration in phase D, a hydrous phase capable to store up to 18 wt% H_2O, theoretically, much more than serpentine minerals.

METHODS

Multi-Anvil Synthesis Experiments

The starting materials used to synthesize minerals in this study consisted in mixtures of high purity oxide powders MgO (99.998%) and SiO_2 (99.998%) that were dehydrated in an oven at 1,000–1,100°C overnight prior to weighing. Iron was incorporated in the mixture as FeO (99.5%), and water was incorporated by adding brucite, $Mg(OH)_2$ (95%, the rest being adsorbed CO_2), and in some experiments by adding additional distilled H_2O (see **Table 1**). Four compositions were prepared: two Fe-free Mg_2SiO_4 and two Fe-bearing (Fo90) compositions containing 5 and 10 wt% H_2O, respectively. The weighed oxides and hydroxides were ground in ethanol for 1 h, dried under an IR lamp and then stored in a vacuum furnace until loading. The starting materials were embedded in $Au_{80}Pd_{20}$ capsules and when Fe-bearing mixtures were employed an additional Re inner capsule was used to avoid iron loss. In some experiments, two capsules were loaded together, and these are referred to as *a* and *b*.

The high-pressure (HP) and high-temperature (HT) syntheses were performed in a multi-anvil press installed at Laboratoire Magmas et Volcans (LMV), Clermont-Ferrand (France) using Cr-doped MgO octahedral assemblies of 14 mm edge for experiments at 14 GPa and 10 mm edge for those run at higher pressures. We used tungsten carbide cubes with 8 and 4 mm truncations, respectively, and the pressure calibration previously described by Boujibar et al. (2014) was followed. Heating and thermal insulation of the experimental charge were ensured by a $LaCrO_3$ furnace and a ZrO_2 sleeve, respectively. To protect the samples from La and Cr contamination, MgO sleeves were placed between the furnace and the capsule. Temperature was monitored during the duration of the experiments (30 min to 5 h, see **Table 1**) with a $W_5Re/W_{26}Re$ thermocouple.

Electron Probe Micro Analysis

After the experiments, the samples were prepared as doubly polished sections cut parallel to the longest dimension of the capsule. The samples were carbon coated for electron probe microanalysis (EPMA). These analyses were performed using a Cameca SX100 installed at LMV, to determine the chemical composition (Mg, Si, and Fe content) of minerals that crystallized in the HP-HT experiments. The standards used in the analyses were wollastonite (for Si), forsterite (for Mg) and fayalite (for Fe) and operating conditions were 15 keV and 15 nA with 20 s

TABLE 1 | Experimental details of sample synthesis and phases produced.

Run No.	P (GPa)	T (°C)	Time (h)	System	Bulk H_2O content (wt%)	Run products
238	19	1,300	2	MSFH	5	γ + sB
224	19	1,400	1	MSFH	5	γ
253	19	1,550	1	MSH	5	γ + L
271	19	1,550	1	MSFH	5[#]	γ + L
231	19	1,600	1	MSFH	5	γ [$]
487	22	1,300	0.5	MSH	10	γ
369a	∼21	1,220	3	MSH	10	γ
369b	∼21	1,220	3	MSFH	5[#]	γ
384a	∼21	1,375	3	MSH	10	γ + St
384b	∼21	1,375	3	MSFH	5[#]	γ
367	∼21	1,300	3	MSFH	5[#]	γ
365	∼21	1,500	2.5	MSFH	5	γ
362	∼21	1,550	2.5	MSH	5	γ + L
385	∼21	1,700	1	MSH	5	γ + L
2053*	18	1,200	5	MSH	5	β + L
2054*	17	1,200	5	MSH	5	β + L
382	∼15	1,200	3	MSFH	5[#]	β
380a	∼15	1,250	3	MSH	10[#]	β
380b	∼15	1,250	3	MSFH	5[#]	β
377	∼15	1,300	3	MSFH	5[#]	β
269	19	1,350	2	MSH	20	β+sB+Cen+St+L
268	19	1,450	2	MSH	10	β + L
226a	16	1,500	3	MSH		β + L
230a	16	1,500	3	MSH		β
226b	16	1,500	3	MSFH		β + α
267	19	1,650	1	MSH	5	β + L
280	19	1,400	2	MFSH	5	D+sB+melt
388	21	1,200	3	MSH	15	D+sB+melt
485	21	1,180	1	MSH	10	D+sB+melt
488	22	1,200	1	MSH	10	D+sB+(Br)[$]

*α, olivine; β, wadsleyite; γ, ringwoodite; L, liquid/melt phase; sB, superhydrous B; D, phase D; St, stishovite; Br, brucite; Cen, clinoenstatite. *experimental charges from Demouchy et al. (2005). [#]distilled H2O was added to the capsule starting mixture. [$]traces of brucite found at one end of the capsule.*

counting time (10 s on the peak and 10 s on the background). The results of the analyses are given in **Tables 2**, **3**.

Elastic Recoil Detection Analysis (ERDA)

ERDA analyses were performed using the nuclear microprobe of Laboratoire d'Etude des Eléments Légers, CEA, Saclay, (France) following the set up by Khodja et al. (2001). The detailed analytical procedure is described in detail in Raepsaet et al. (2008) and Bureau et al. (2009) and this technique has been successfully used in a number of recent studies to determine H contents in NAMs (Withers et al., 2012; Novella et al., 2014). The measurements were performed through three different sessions. The samples were gold coated in the first session and carbon coated in the following ones. The metal used for coating has no effect on the measurement of the water content, but we found that Au coating induces a low energy tail in the ERDA spectrum that is difficult to fit. A 3 MeV $^4He^+$ beam was produced by a single stage Van de Graaff accelerator and focused on a 3 × 3 μm² or 2 × 2 μm² surface using quadrupole magnetic lenses. The analysis then utilizes three detectors at the same time: an X-ray detector to record particle induced X-ray emissions, an annular detector to record Rutherford back-scattered (RBS) particles, and an ERDA detector to record H atoms ejected from the sample through elastic collisions with the alpha particles.

The samples and standards may be tilted such that the polished surface is oriented either perpendicular to the beam in the standard Rutherford-backscattering analysis geometry, or at a low "grazing" angle of 15° from the incident beam for the ERDA configuration as the dedicated detector is located at 30° relative to the incident beam direction. The beam size on the sample surface was 12 × 3 μm^2 in the ERDA configuration, and the beam was scanned over the sample surface to produce compositional maps. Forward scattered incident He particles were prevented from reaching the ERDA detector by placing a 15 μm Al foil in front of the detector. At the beginning of each session, the standards were analyzed in the RBS geometry to determine the RBS solid angle (Ω_{RBS}).

Standards such as Al_2O_3, FeS_2, SiO_2, $CaCO_3$, SnBi, Zr, ZrH, and Kapton are used to calibrate the RBS solid angle. Analysis time was 15 min for each standard, except for the Kapton (30 min). The SIMNRA program (Mayer, 1999) was used to model RBS and ERDA energy spectra. The average solid angle, Ω_{RBS}, thus determined was 73.12 ± 9.72 in the first session, 66.4 ± 3.26 in the second session and 59.53 ± 3.09 in the third session. The ERDA solid angle (Ω_{ERDA} = 16.66 mSr in the first session, 15.59 ± 0.54 mSr in the second session and 8.47 mSr in the third session) was calibrated from a 3,700 s analysis in ERDA configuration of the Kapton standard, but also of ZrH standard in the second session (Wang, 2004). The RBS spectrum allows the quantification of the charge on the sample during the course of the ERDA measurement. The Kapton standard was assumed to be stoichiometric $C_{22}H_{10}O_5N_2$.

The samples were analyzed in the ERDA configuration with analysis times that varied between 20 and 120 min. An area of the sample was scanned with the beam (**Figure 1A**). Using the RISMIN software (Daudin et al., 2003), areas can be selected within the analyzed map to avoid cracks, grain boundaries or secondary mineral phases (see **Figure 1B**). The H contents of the samples were calculated by simulation of the ERDA spectra using the SIMNRA program. Knowing the composition of the sample, the RBS spectra were fitted in order to monitor the charge, a necessary input to calculate the bulk water content from the ERDA spectrum (see **Figure 1C**). The thickness of the gold coating (8 to 9 nm, corresponding to 48 × 10^{15} atom cm^{-2}) or of the C coating (∼100 × 10^{15} atom.cm^{-2}) was determined for each analyzed area from the RBS spectra, and the surface hydrogen was modeled as a single layer of H atoms that varied between 16 × 10^{15} and 47 × 10^{15} atom.cm^{-2}. The principal source of uncertainty in H contents is derived from the detector counting statistics. Additional minor sources of uncertainty include contributions from uncertainties in sample tilt angle, RBS solid angle and ERDA energy calibration. Uncertainties

TABLE 2 | Chemical composition of wadsleyite and ringwoodite samples from EPMA (oxides in wt% and atoms per formula unit) and ERDA (H in wt% H_2O).

	SiO_2		MgO		FeO		Total		H_2O		(Mg+Fe)/Si		Si		Mg		Fe		H	
WADSLEYITE																				
230A	40.963	0.470	49.238	0.200	10.092	0.250	100.293	0.660	0.132	0.011	1.998	0.023	0.994	0.012	1.780	0.007	0.205	0.004	0.021	0.002
226A	41.788	0.510	50.316	0.350	8.075	0.490	100.179	0.770	0.467	0.044	1.957	0.018	0.990	0.011	1.776	0.013	0.160	0.010	0.074	0.007
382	41.439	0.271	46.941	0.390	7.685	0.132	96.065	0.567	1.671	0.064	1.844	0.014	0.964	0.006	1.627	0.014	0.149	0.003	0.259	0.010
380B	40.866	0.335	48.239	0.580	8.877	0.259	97.982	0.815	1.220		1.941	0.020	0.955	0.008	1.681	0.020	0.174	0.005	0.190	
377	40.431	0.303	49.028	0.339	10.137	0.319	99.596	0.530	0.155		2.018	0.010	0.986	0.007	1.782	0.012	0.207	0.007	0.025	
226B	42.484	0.580	56.530	0.660	0.084	0.030	99.098	0.930	0.378		1.986	0.033	0.985	0.014	1.955	0.022	0.002	0.000	0.058	
267	42.386	0.186	55.803	0.302	0.035	0.026	98.224	0.354	0.347		1.963	0.014	0.994	0.004	1.951	0.011	0.001	0.000	0.054	
268	42.468	0.224	54.667	0.395	0.024	0.028	97.159	0.425	0.846	0.039	1.920	0.019	0.983	0.006	1.886	0.014	0.000	0.000	0.131	0.006
269	42.667	0.107	56.844	0.121	0.010	0.017	99.522	0.152	0.081		1.986	0.006	1.000	0.003	1.987	0.004	0.000	0.000	0.013	
2054	43.494		52.120		0.003		95.617		3.107	0.083	1.786		0.919	0.000	1.642		0.000		0.438	0.012
2053	43.558		53.198		0		96.756		2.109	0.008	1.821		0.954	0.000	1.737		0.000		0.308	0.001
380A	42.363	0.260	54.341	0.329	0.798	0.249	97.502	0.531	1.011		1.928	0.012	0.972	0.006	1.858	0.011	0.015	0.005	0.155	
RINGWOODITE																				
224	40.753	0.110	48.225	0.380	10.244	0.750	99.223	0.510	0.326	0.032	0.991	0.003	1.748	0.015	0.208	0.000	0.208	0.000	0.053	0.005
271	41.481	0.394	3.471	0.683	52.682	0.242	97.634	0.664	0.429	0.042	0.989	0.010	1.873	0.024	0.069	0.000	0.069	0.000	0.068	0.007
231	41.114	0.133	48.506	0.373	9.355	0.105	98.975	0.505	0.517	0.050	1.948	0.012	0.990	0.003	1.739	0.013	0.188	0.001	0.083	0.008
238	41.449	0.234	48.215	0.385	10.736	0.310	100.400	0.529	0.440	0.053	1.951	0.013	0.993	0.006	1.722	0.014	0.215	0.006	0.070	0.009
384A	40.774	0.306	49.243	0.439	9.315	0.024	99.332	0.735	0.155		1.992	0.005	0.994	0.007	1.790	0.016	0.190	0.000	0.025	
365	40.429	0.283	48.806	0.575	10.086	0.577	99.321	0.604	0.023		2.008	0.015	0.996	0.074	1.792	0.021	0.208	0.012	0.004	
369B	41.116	0.319	49.516	0.263	8.696	0.356	99.328	0.567	0.165	0.005	1.972	0.013	1.000	0.008	1.796	0.010	0.177	0.007	0.027	0.001
367	40.361	0.400	48.423	0.480	9.595	0.167	98.379	0.860	0.458	0.094	1.987	0.021	0.979	0.010	1.752	0.017	0.195	0.003	0.074	0.015
384B	42.675	0.262	55.462	0.305	0.039	0.255	98.175	0.505	0.628	0.018	1.938	0.005	0.988	0.007	1.914	0.015	0.001	0.000	0.097	0.003
385	42.756	0.266	55.167	0.302	0.147	0.030	98.070	0.485	0.885		1.926	0.012	0.979	0.006	1.883	0.010	0.003	0.000	0.135	0.000
369A	42.616	0.381	55.432	0.574	0.743	0.512	98.790	0.711	0.409	0.082	1.954	0.012	0.994	0.009	1.928	0.020	0.014	0.010	0.064	0.013
362	42.492	0.290	54.774	0.287	0.033	0.035	97.300	0.464	1.038	0.025	1.922	0.013	0.972	0.007	1.868	0.010	0.001	0.001	0.159	0.004
253	43.505	0.420	55.131	0.460	0.000	0.000	98.680	0.770	1.164	0.111	1.890	0.016	0.978	0.009	1.847	0.015	0.001	0.000	0.175	0.017
487	42.39	0.269	54.349	0.585	0	0	96.739		1.832			0.010	0.937	0.005	1.791	0.020			0.270	

associated with cross sections and stopping powers used by SIMNRA are minor and were not taken into account. "Surface H" and "bulk H" maps were produced by plotting respectively the number of detector events recorded with energies in the high and low energy regions of the ERDA spectrum. Maps of Au and major elements (Fe, Mg, Si, O, and combinations thereof) were produced from the corresponding energy steps in the RBS spectra. The regions of the analyses used for quantification of H excluded the areas of any surface features that result in anomalies in the Au, H and major element compositional maps but also capsule material as shown in **Figure 1B**.

A typical ERDA energy spectrum is shown in **Figure 2**. The intense signal at high energy represents H atoms that have been ejected from the surface of the sample and that arrive at the detector with high energy (**Figure 2A**). The energy of an alpha particle decreases as the sample is penetrated, so particles that originate from within the sample arrive at the detector with correspondingly lower energy, as represented by the lower energy plateau in the ERDA spectrum. Surface pollution of the sample can therefore be easily distinguished from bulk content, and it is through simulation of the low energy plateau in the ERDA spectrum that the H content of the sample itself is calculated. The bulk H signal was calculated using the integration of the signal between 200 and 500 keV. The signal remained stable throughout the duration of the analyses, showing that the signal is not modified by beam exposure (Bureau et al., 2009).

Infrared Spectroscopy

Polarized and unpolarized Fourier Transform infrared spectra were acquired using a Vertex70 Bruker spectrometer coupled to a Hyperion microscope equipped with ×15 objective and condenser at LMV. Beam size in the analyses varied from 30 to 50 μm depending on the size of the crystals and the presence of cracks/inclusions. The spectra were collected through a CaF_2 plate with a resolution of 2 cm^{-1} and with up to 300 scans. After application of a linear baseline with anchor points outside the OH stretching region, the absorbance was integrated from 3,200 to 3,650 cm^{-1} for wadsleyite and 2,000 to 3,730 cm^{-1} for ringwoodite. The absorption coefficient was then quantified using the Beer-Lambert law:

$$A = \varepsilon.c.t$$

where A is the absorbance, ε is the absorption coefficient in $L.mol^{-1}.cm^{-2}$, c is the concentration in moles H_2O/L and t is the thickness in cm. Density factors required in order to convert water concentrations from ppm weight H_2O into moles of H_2O/L were calculated for wadsleyite and ringwoodite using crystallographic data from several sources (see **Table 4**). Thickness of the samples was accurately measured either using a Mitutoyo micrometer or the microscope of a Renishaw Raman spectrometer, with uncertainties in thickness measurements of the order of 1–3 μm on average.

For orthorhombic wadsleyite, the water quantification was based on the average of ∼10 unpolarized measurements performed on randomly oriented grains within the doubly polished thin sections. The absolute absorbance of the crystal

TABLE 3 | Composition of Phase D as measured with electron microprobe and ERDA for water.

	Oxide wt%								Atoms					
Run#	SiO_2	MgO	FeO	Total	H_2O		(Mg+Fe)/Si	Si	Mg	Fe	H			
280	59.339	0.415	23.696	0.224	3.842	0.198	86.877	0.542	11.2	1.1	0.565	0.008	0.988	0.007	0.588	0.006	0.053	0.003	1.247	0.125
388	63.055	0.618	24.668	0.363	0.000	0.000	87.723	0.981	9.1	0.9	0.586	0.009	1.049	0.010	0.612	0.009	0.003	0.001	1.011	0.101
484	60.783	0.770	22.860	0.458	0.000	0.000	83.642	1.215	11.0	1.1	0.561	0.005	1.012	0.013	0.567	0.011	0.000	0.000	1.221	0.122
485	62.049	0.189	23.421	0.331	0.000	0.000	85.470	0.142	8.6	0.9	0.563	0.010	1.033	0.003	0.581	0.008	0.000	0.000	0.957	0.096
488	60.555	0.340	24.578	0.239	0.000	0.000	85.133	0.536	6.7	0.7	0.605	0.004	1.008	0.006	0.610	0.006	0.000	0.000	0.745	0.075

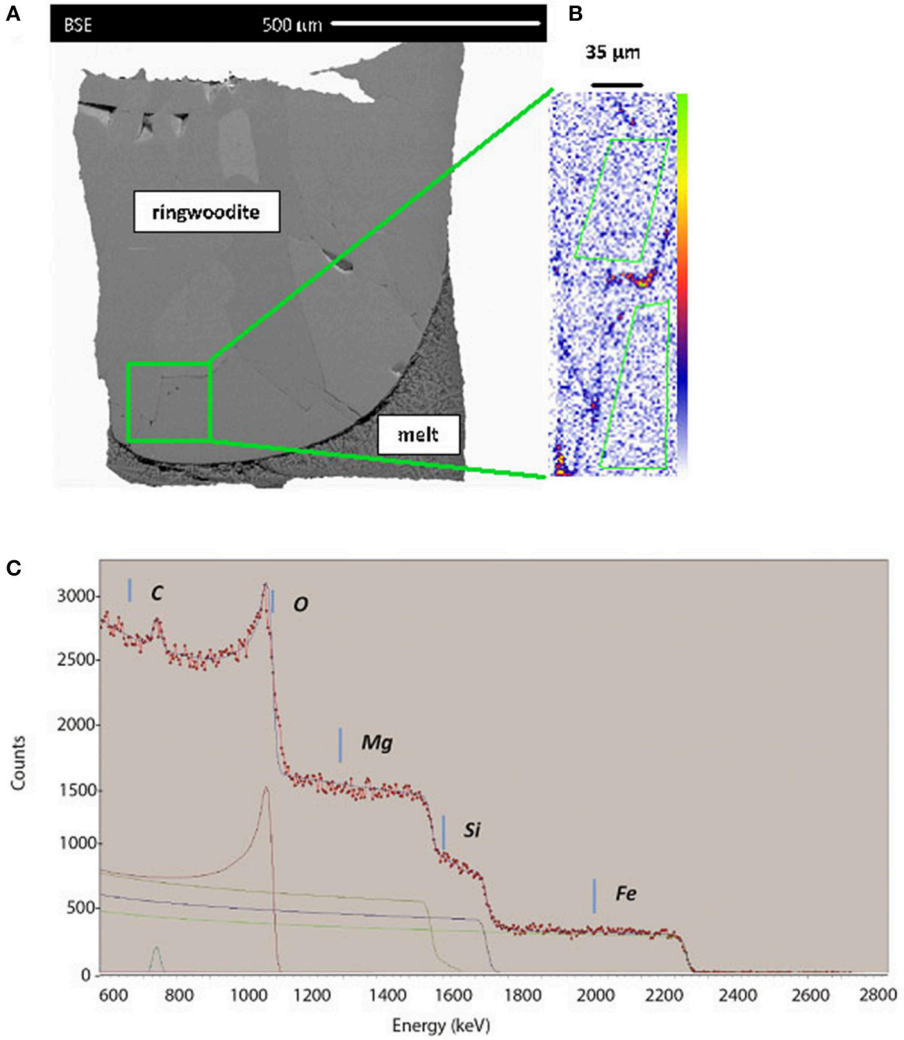

FIGURE 1 | (A) Backscattered electron image of a ringwoodite sample, with the green rectangle corresponding to the area analyzed by ERDA. **(B)** H map collected for the selected area. The green polygons define the regions within the crystal that were selected for integration to get the final RBS and ERDA spectra. **(C)** RBS spectrum. The blue curve represents the fit to the data (in red). The different lower curves represent the intensity in each element as specified (C, O, Mg, Si, Fe). The composition being constrained by the EPMA, the intensity of the spectrum allows calculating the charge on the sample.

is then equal to three times the average of the unpolarized measurements as demonstrated by Kovacs et al. (2008) and Bali et al. (2008). The error associated with the use of unpolarized radiation was estimated by Sambridge et al. (2008) to be 20% of the absolute absorbance if 10 grains are used. Given that the anisotropy of OH absorption in wadsleyite is less than in olivine (see Jacobsen et al., 2005; Bali et al., 2008; Deon et al., 2010), the error here should be less when applying unpolarized radiation on wadsleyite than on olivine.

RESULTS

Phase Compositions and Water Contents

The composition of wadsleyite and ringwoodite crystals are shown in **Figure 3**. The Mg/Si or (Mg+Fe)/Si ratios as measured by EPMA are observed to decrease with increasing water content as determined by ERDA, in agreement with the observations of Inoue et al. (1995) using Secondary ion Mass Spectrometry (SIMS). We also observe that determination of water content using EPMA totals overestimates water contents by 1–2 wt% H_2O compared to quantification based on ERDA. Also, there is more scattering when plotting (Mg+Fe)/Si ratios vs. EPMA weight totals, indicating that using the EPMA totals below 99–101 wt% is less precise for determining water contents than the ERDA method (**Figures 3A**,**B**). The trend in (Mg+Fe)/Si ratio vs. water content does not depend on the presence of iron in neither wadsleyite, nor ringwoodite, thus we neglected the ferric iron species when calculating the molar concentration of H (see **Table 2**). Moreover, we do not observe a change in the infrared OH absorption bands with the incorporation of iron. The Fe^{3+} content of wadsleyite under oxidizing conditions is

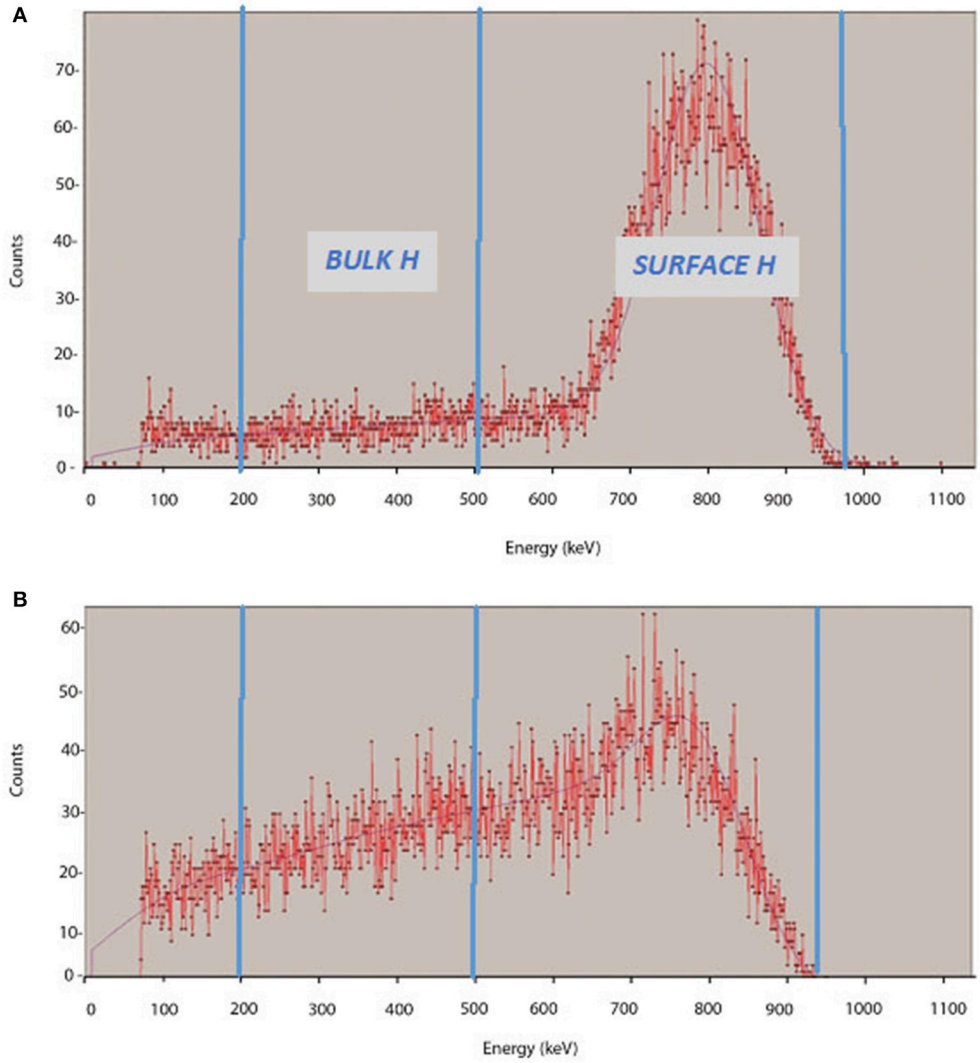

FIGURE 2 | ERDA spectra of two samples with different water concentrations **(A)** 369b ringwoodite with 0.16 wt% H_2O and **(B)** 362 ringwoodite with 1.03 wt% H_2O. The contribution from surface H is evidenced by the strong peak at high energy. The bulk H content of the crystal is calculated from integration of the signal between 200 and 500 keV.

at most 30% Fe^{3+}/Fe_{total}, see Bolfan-Casanova et al. (2012), hence here it would correspond to an amount of at most twice 0.03 error in H for a Fo90 composition. In samples synthesized under similar conditions (Mrosko et al., 2013) report low Fe^{3+}/Fe_{total} ratios in ringwoodite, usually below 10%.

SIMS and ERDA data for wadsleyite are comparable but SIMS values display a higher dispersion as shown in **Figure 3**: for example sample 2054 measured with SIMS by Demouchy et al. (2005) was reported to have 1.24 wt% H_2O, while we find here 3.1 wt% H_2O using ERDA, which is in good agreement with the (Mg+Fe)/Si ratios vs. H_2O wt% trend. Demouchy et al. (2005), reported this experiment as unreliable in terms of water content and Mg/Si, but we believe that its water content, as we measured by ERDA, is correct, even if almost 3 times higher than reported by SIMS.

As in previous studies in Mg_2SiO_4+H_2O system, we observe that at low temperature in the olivine-water system, phase D [$MgSi_2O_4(OH)_2$] coexists with brucite + superhydrous phase B, and as temperature increases, superhydrous phase B + melt (Frost and Fei, 1998; Ohtani et al., 2000; Ganskow and Langenhorst, 2014). Phase D and superhydrous phase B grow as an intimate mixture in the Mg_2SiO_4-water system (Frost, 1999), and only phase D could be analyzed using ERDA because large crystals grew at the interface with the silicate melt. The analysis totals vary between 83 and 88 wt%, indicating large variations in water content [the composition $MgSi_2O_4(OH)_2$ corresponds to a theoretical water content of 18 wt% H_2O, hence a theoretical weight total of 82%]. In this study, phase D displays a variable composition with Mg/Si ratio between 0.56 and 0.65, within the range reported in the literature (0.55 and 0.77, see Frost and Fei, 1998; Ohtani et al., 2000; Ganskow

TABLE 4 | Results of the Infrared analyses used to calculate the absorptivity coefficients for wadsleyite and ringwoodite.

	nbr grains	Area (cm²)	σ	c (ppm wt H_2O)	X[a]	t (μm)	σ	ε [L/(molH_2O*cm-^{2})]	σ	Fe#
WADSLEYITE										
269	10	44.90	3.43	806	5,181	119	12	72,771	5,854	0
226A	12	117.85	13.26	4,000	5,181	67	8	65,176	7,309	0
Average for Fo100								**68,973**	6,582	0
226B	9	119.43	9.29	4,209	5,029	67	8	**67,238**	5,230	8.3
230	11	17.41	3.60	1,322	4,992	26	6	**75,641**	15,736	10.3
RINGWOODITE[b]										
224	6	439.46	30.37	3,259	4,885	142	3	139,166	9,616	10
238	4	370.00	22.50	4,400	4,885	94	3	131,100	7,971	10
271	4	319.62	15.53	4,289	4,998	85	2	**131,453**	6,389	3
362	3	570.51	19.23	10,380	5,067	71	3	117,674	3,966	0
253	4	612.39	35.15	11,638	5,067	67		119,385	6,853	0
Average for Fo100								**118,529**	5,409	0
Average for Fe90								**135,133**	8,794	10

[a] *The conversion parameter (from ppm wt H_2O to mole H_2O/L) was calculated using densities as retrieved from Horiuchi and Sawamoto (1981) cell parameters for pure Mg_2SiO_4 and the data from Finger et al. (1993) for Fe-rich wadsleyites. For ringwoodite, cell parameters from Finger et al. (1993) and Ganskow et al. (2010) were used.*
[b] *The area of integration for ringwoodite here includes the 2,500 cm^{-1} band. The data in bold is the one used in **Figures 6**, **7**.*

and Langenhorst, 2014; Ghosh and Schmidt, 2014). The water content of phase D as determined by ERDA varies from 6.7 to 11.2 wt% H_2O, very different from the water content calculated from the EPMA weight totals of 83–87 wt%, that is 13–17 wt% H_2O, see **Table 3.**

Infrared Spectra and Bands Assignment

The averages of nine to twelve unpolarized infrared spectra of wadsleyites are shown in **Figure 4** (see also **Supplementary Figure 1**) as measured on four different samples. We identified up to nine OH absorption bands: three weak bands at 3,692, 3,260, and 3,472 + 3,428 cm^{-1}, three strong bands at 3,400–3,350, ∼3,320 and 3,300 cm^{-1}, and two bands at 3,613 and 3,580 cm^{-1}, and a very weak band around 3,000 cm^{-1} observed in H-poor wadsleyite. Compared to the spectra reported by Jacobsen et al. (2005), those in this study display an additional band at 3,400 cm^{-1}, which was observed in the study of Kohn et al. (2002). The bands at 3,613 and 3,580 cm^{-1}, and also the two weak bands at 3,428 and 3,472 cm^{-1}, seem to appear at high water contents (here above 800 ppm wt H_2O).

The spectra of ringwoodite are shown in **Figure 5**, where the average of four to six unpolarized spectra recorded on different grains is shown. The spectra display the typical very broad band at 3,117 cm^{-1}, accompanied of weaker satellite bands at 3,687 + 3,733 cm^{-1} and 2,538 + 2,441 cm^{-1}. A shoulder of the main band located at 3,210 cm^{-1} is detected in some samples and a very weak feature at 3,550 cm^{-1} is observed in some iron-bearing samples. Sometimes a band at 2,666 cm^{-1} is observed as well as a feature at 2,364 cm^{-1}. The samples are homogeneous, judging from the similarity of the spectra (ringwoodite is cubic, hence no pleochroism should be observed for the absorption bands of structural OH).

Interpretation of spectroscopic data is not always straightforward in terms of site occupancy. For example, Smyth et al. (2003) noticed that the frequency of the main OH band at ∼3,117 cm^{-1} in the infrared spectrum of ringwoodite would correlate with a distance of 2.7 Å, rather in the range of O-O distances found for the tetrahedral edge (2.71 Å) than for the octahedral edges (2.86–2.31 Å). But it is not easy to use the distance-frequency (i.e., d_{O-O} vs. ν_{OH}) correlation (see Libowitzky, 1999) as it is influenced by the angle made by the O-H and H…O bonds. More recently, Ganskow et al. (2010) and Mrosko et al. (2013) assigned the main band at 3,117 cm^{-1} to H coupled to Mg vacancies because they observed that this band shifts to higher wavenumbers when iron content of the ringwoodite increases. This observation is in agreement with the expansion of the octahedron upon the incorporation of larger iron cations and with the positive correlation between O…O interatomic distances and OH frequencies (Libowitzky, 1999). Mrosko et al. (2013) assigned the 3,700 cm^{-1} band to H in the tetrahedron, in agreement with Blanchard et al. (2009), based on the fact that this band shifts to lower wavenumbers when iron content increases. This would imply that the tetrahedron shrinks upon iron incorporation, which is not the case (see Hazen et al., 1990; Smyth et al., 2014), or that the O-H…O bond angle varies. They also observed a band at 3,420 cm^{-1} which is attributed to H coupled to Mg substituted to Si in tetrahedral sites. Concerning the group of bands at ∼2,500 cm^{-1} its assignment to OH stretches remains controversial. Hofmeister and Mao (2001) interpreted this band as a combination of overtones of Si-O related vibrations, however we insist on the fact that their sample contained water (as can be seen on their spectra) and also on the fact that this band is extremely weak in H-poor samples as observed by Bolfan-Casanova et al. (2000). If indeed, due to an OH stretch, the frequency of the bands at ∼2,500 cm^{-1} corresponds to 2.6 Å, in agreement

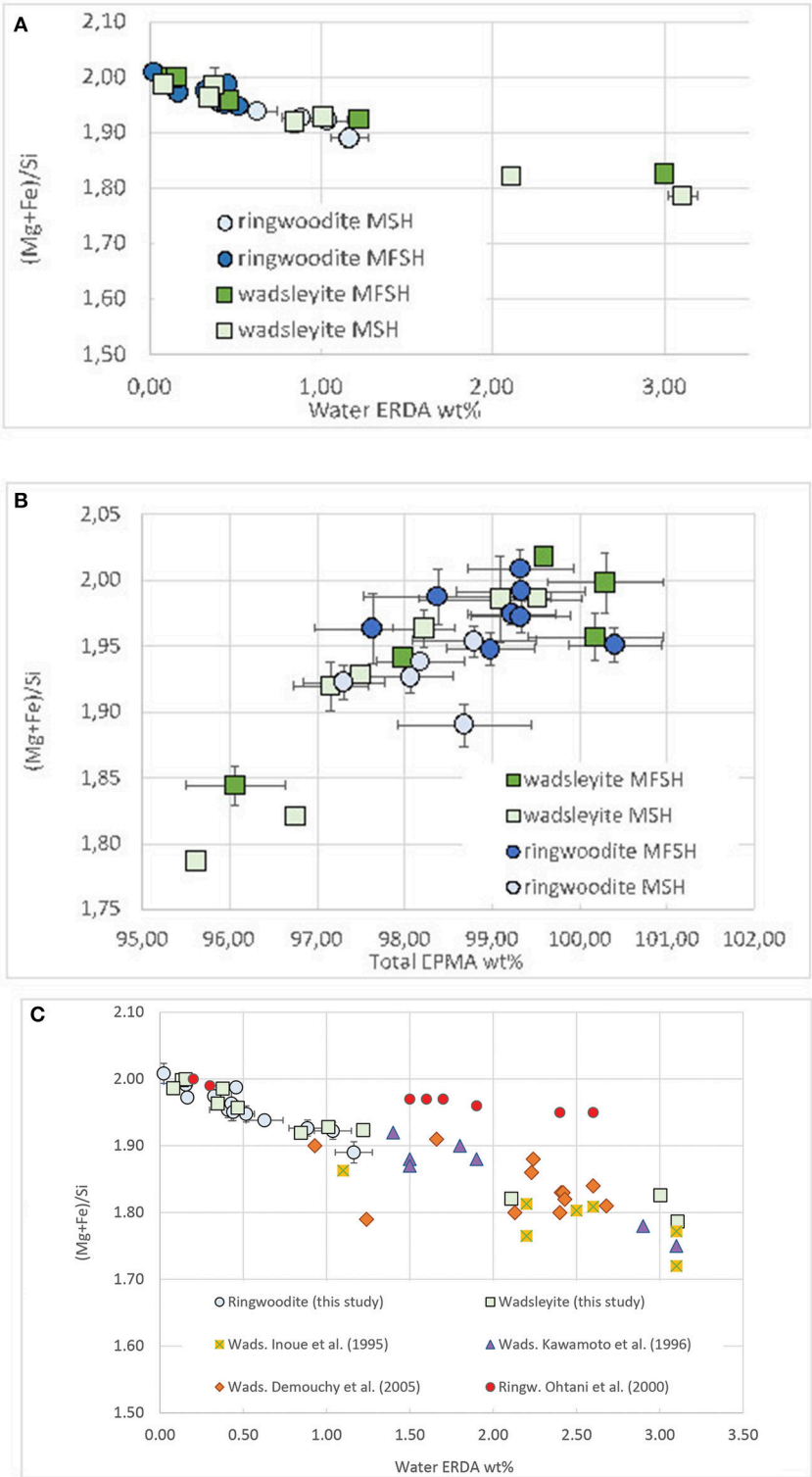

FIGURE 3 | Electron probe micro analyses of wadsleyite and ringwoodite samples from this study in the MSH and MFSH systems. We do not observe any specific effect of the presence of iron. **(A)** The (Mg+Fe)/Si ratio as a function of water content as measured by ERDA. **(B)** The same ratio as a function of EPMA weight totals. This plot evidences the lack of precision of EPMA analysis totals to measure quantitatively water contents. **(C)** (Mg+Fe)/Si ratio compiled for all systematic studies, showing a satisfying agreement between SIMS and ERDA data for wadsleyite, but not for ringwoodite at high water contents. All previous studies were focused on wadsleyite samples, except that of Ohtani et al. (2000) focusing on ringwoodite samples.

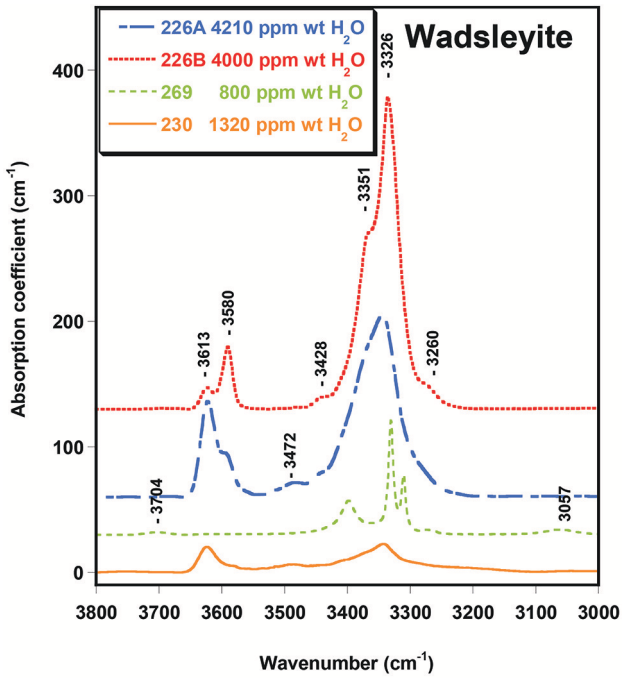

FIGURE 4 | Averages of unpolarized spectra of four wadsleyite samples containing different water contents (the number of spectra used for averaging is shown in **Table 4**).

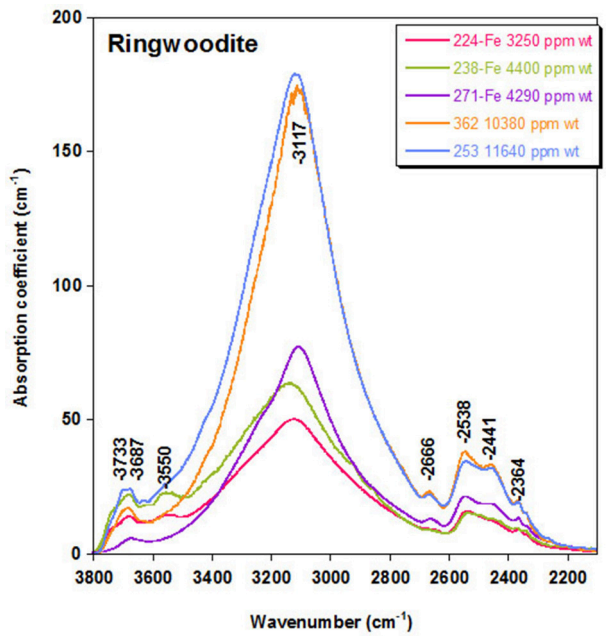

FIGURE 5 | Infrared spectra of ringwoodites synthesized in this study with different water contents. The absorbance was integrated using the range [2,200–3,700] cm^{-1}. The samples containing iron are indicated.

with bond distances found in the tetrahedron (Libowitzky, 1999).

Infrared Extinction Coefficients for OH Bands in Wadsleyite and Ringwoodite

The extinction coefficient or molar absorptivity can be recalculated from Beer-Lambert law, knowing the absorbance, the concentration of water (independently determined by ERDA in this study) and the thickness. Concerning wadsleyite, knowing the water content of the sample and the average of unpolarized absorbance, multiplied by three (see Kovacs et al., 2008), yields the molar absorptivity or extinction coefficient. We measured four different wadsleyite samples, with water contents ranging from 800 to 4,200 ppm wt (**Table 4**, **Figure 6**) and we observe no effect of water content on the absorptivity. The average for the two iron free samples leads to an absorptivity of 69,000 ± 7,000 L/moles H_2O/cm^2, in excellent agreement with the value of 73,000 ± 7,000 L/moles H_2O/cm^2 determined by Deon et al. (2010). The absorptivity for the samples containing 8 to 10 mole% Fe is 67,000 ± 5,000 and 75,000 ± 15,000 L/moles H_2O/cm^2, respectively, very similar to values for the Mg end-member and virtually the same when considering uncertainties.

The molar absorptivity of ringwoodite was calculated separately from the FTIR analysis performed on 5 different samples (**Table 4**). The absorptivity values vary from 118,000 ± 4,000 for sample #362 (with no Fe) to 139,000 ± 9,000 for #224 (with 10% mole Fe). The error bar on each absorptivity value is calculated from the standard deviation determined from measurements on different grains of the same sample, and amounts to approximately 6%. We do not observe an effect of iron content on the absorptivity coefficient unlike what Koch-Muller and Rhede (2010) observed for ringwoodites containing between 40 and 100 mole% Fe. For example, the sample containing 3% FeO here displays an absorptivity of 131,000 ± 6,000 L/moles H_2O/cm^2, similar to that of the samples containing 10% FeO: 135,000 ± 9,000 L/moles H_2O/cm^2 (see **Figure 6**). Based on the data presented here we propose an absorptivity of 118,000 ± 5,000 for Fe-free ringwoodite and 135,000 ± 9,000 for Fe-bearing (Fo90) ringwoodite. Our value of ε for Fe-free ringwoodite is 15% higher than that extrapolated by Koch-Muller and Rhede (2010) and 10% higher than the more recent value determined using proton-proton scattering from Thomas et al. (2015). Indeed, Thomas et al. (2015) did not take into account the infrared feature at 2,500 cm^{-1}, which we did. We also tested calculating ε without taking into account this band in the integration of the absorbance and differences correspond to a maximum of 11%, thus explaining the 10% difference between the ε value from Thomas et al. (2015) and from the current study.

If we calculate the water content of the ringwoodites using the absorptivity coefficient of Paterson (1982), we find that the water contents are about approximately 50% lower than the water contents determined by ERDA ($[H_2O]_{Paterson}/[H_2O]_{ERDA} \sim 0.55 \pm 0.02$). This ratio between water contents determined using Paterson (1982) and those measured using ERDA can also be estimated graphically on **Figure 7** for any wavenumber.

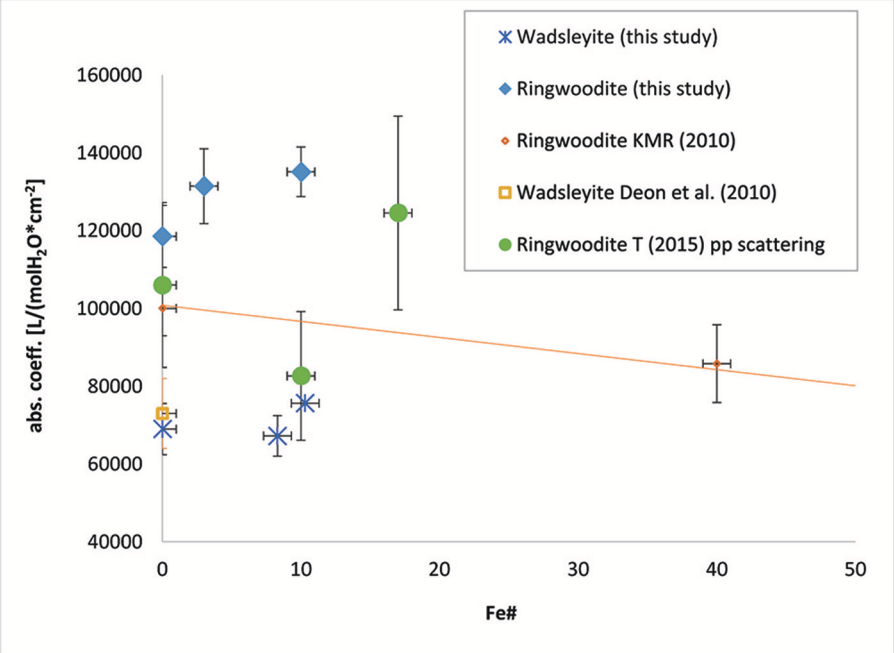

FIGURE 6 | Absorptivity coefficient (ε) measurement for wadsleyite and ringwoodite of this study as a function of the iron content, and compared to previous determinations. KMR stands for Koch-Muller and Rhede (2010) and T. for Thomas et al. (2015). Note that the value of KMR for iron-free ringwoodite is interpolated from values measured on samples with different iron contents (not shown). Within the error bar, we do not observe an effect of iron on the value of ε.

DISCUSSION

Incorporation of Water in Wadsleyite and Ringwoodite

In this study we observe the same decrease in (Mg+Fe)/Si atomic ratio as a function of water content (measured by ERDA) for wadsleyite and ringwoodite. This trend compares well with those established by Inoue et al. (1995), Kawamoto et al. (1996), and Demouchy et al. (2005) for wadsleyite, that used SIMS to measure water contents. However, the behavior reported by Ohtani et al. (2000) for ringwoodite (using SIMS as well), indicates that more H substitutes for Si sites in this phase than in its lower pressure polymorph (see **Figure 3C**).

The trend first observed by Inoue et al. (1995) and also observed in this study is consistent with two H atoms substituting for one octahedral Mg in wadsleyite, $(2H)^{x}_{Me}$ in Kröger-Vink notation (Kröger and Vink, 1956). This is in agreement with the predictions of Smyth (1994) based on electrostatic considerations that shed light on the under-bonded character of the O1 oxygen of wadsleyite (the only one not bonded to a silicon atom) and that makes it the best candidate for protonation. This H incorporation mechanism was in fact later confirmed by X-ray single crystal diffraction (Kudoh et al., 1996, 2000; Smyth and Kawamoto, 1997; Ye et al., 2012), and more recently by neutron powder diffraction (Sano-Furukawa et al., 2011), showing vacancies mainly in the M3 octahedral site of wadsleyite. Also, most infrared features in wadsleyite have been assigned to hydrogen in Mg vacancies by Jacobsen et al. (2005) and Deon et al. (2010), except for the band around 3,000 cm^{-1} that was assigned to H replacing Si, based on its pleochroism and frequency (see also Kohn et al., 2002).

From the electrostatic point of view, ringwoodite was not expected to be a fully hydrated structure since there is no non-silicate bonding oxygen in the structure, as there is in wadsleyite (see Smyth, 1994). Using single crystal X-ray diffraction, Kudoh et al. (2000) observed that, in $Mg_{1.89}Si_{0.98}H_{0.30}O_4$ ringwoodite containing 2 wt% H_2O (as determined by SIMS analyses), the vacancies are mainly located at the Mg site. Still, they realized that the Mg/Si ratio of this ringwoodite was higher (1.95) than that of wadsleyite containing the same water content (1.8); this led them to suggest the coupled substitution 3Mg = 6H and Si = MgH_2 in hydrous ringwoodite, resulting into Mg_2Si = 8H. This Mg-Si disorder could be responsible for the very large width of the band centered at 3,120 cm^{-1} as observed in the IR spectrum of hydrous ringwoodite. On the other hand, Smyth et al. (2003) observed a systematic increase of the size of the octahedral site with H incorporation together with cation occupancy deficiency in this site, whereas the tetrahedral site is nearly full in a series of ringwoodites containing from 0.2 to 1.1 wt% H_2O. Using first principle calculations (Blanchard et al., 2009) interpreted the major absorption band at ∼3,100 cm^{-1} as H located on the O-O edge shared between two octahedra, while the higher frequency band at 3,675 cm^{-1} is attributed to a tetrahedral edge.

More recently, Purevjav et al. (2014) published the first neutron powder diffraction data on ringwoodite with 2.4 wt% D_2O (as determined from the unit cell expansion using the systematics reported in previous reports) and a Mg/Si of 1.93. They concluded to a partial occupancy of the tetrahedral site by

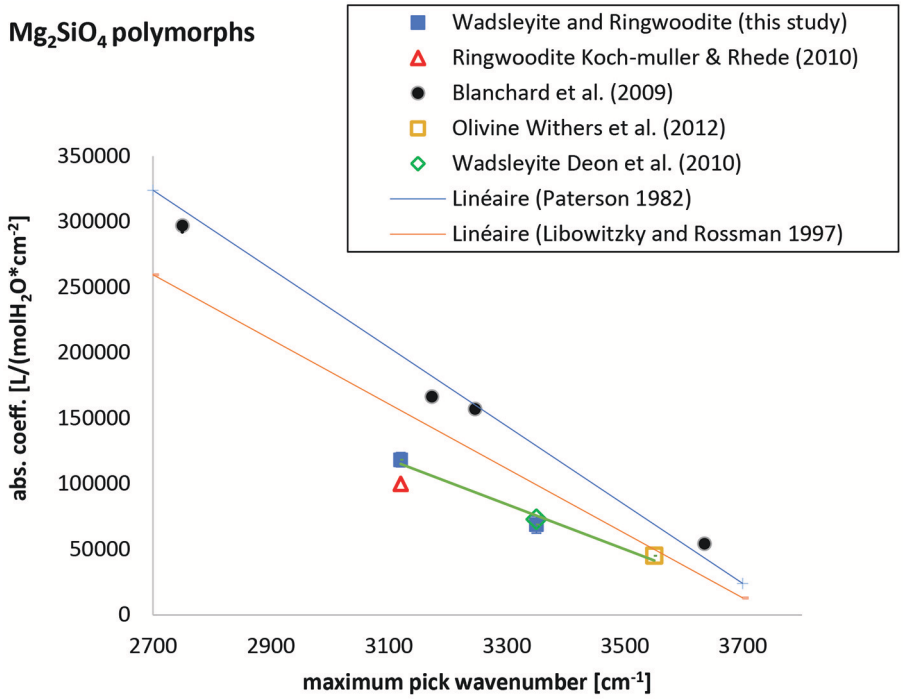

FIGURE 7 | Change in absorptivity coefficient (ε) of the OH band in the infrared as a function of the mean frequency of vibration of the OH (i.e., the latter being represented by the most intense absorption band in the spectrum of the phase of interest). Our value of ε for ringwoodite and wadsleyite agree well with those of Koch-Muller and Rhede (2010) and Deon et al. (2010). We confirm that the experimentally determined ε are lower than the trend of Paterson (1982) but also Libowitzky and Rossman (1997) for wadsleyite and ringwoodite in the latter case.

D. It is suggested that the substitution of silicon by H occurs at elevated water contents (see also Ye et al., 2012). It could be that there is a change in the incorporation mechanism of water in ringwoodite at high water contents. However, at least up to 1.16 wt% H_2O, we observe a trend of Mg/Si in agreement with substitution in the octahedral site, while Ohtani et al. (2000) observe the $Mg_2Si = 8H$ substitution active at 1.5 wt% H_2O. Thus, ringwoodite crystals with higher water contents need to be investigated in order to verify the change in incorporation mechanism.

Incorporation of Water in Phase D

Phase D is of particular interest because it has been proposed as a water carrier down to the lower mantle (Shieh et al., 1998; Ghosh and Schmidt, 2014; Walter et al., 2015). Its wide stability field can be explained by its extended compositional range with large variations in its EPMA weight totals associated to variations of the Mg/Si ratio (see **Figure 8**, 0.55 and 0.77, see Frost and Fei, 1998; Ohtani et al., 2000; Ganskow and Langenhorst, 2014; Ghosh and Schmidt, 2014). Extended solid solution with Al has also been reported, with an aluminum-rich endmember such as $Al_2SiO_4(OH)_2$ being experimentally observed (Pamato et al., 2015). The water content of phase D as determined by ERDA in this study varies from 6.7 to 11.2 wt% H_2O, much lower than the water content recalculated from the EPMA weight totals as explained earlier. These low water contents compared to the expected 18 wt% H_2O of the theoretical end-member $MgSi_2O_4(OH)_2$ can be explained by the high temperatures of synthesis of phase D. In this study we observe that the atomic ratio decreases with increasing water content, in disagreement with previous studies reporting that the Mg/Si ratio negatively correlates with the analyzed totals (see Frost and Fei, 1998, Figure 8 of this study) or the water contents as measured by SIMS by (Ohtani, 1997). Still our compositional range is too limited to conclude, in comparison to previous studies that indeed investigated lower temperatures, as low as 800°C, compared to 1,100–1,400°C here. The compositional range, as proposed by previous authors, arises probably from two incorporation mechanisms (Yang et al., 1997; Frost and Fei, 1998), see **Figure 8**:

$$Si^{4+} = 4H^{+} \text{ and } Si^{4+} = 2H^{+} + Mg^{2+}$$

The compositions shown in **Figure 8** indicate the $Si^{4+} = 2H^{+} + Mg^{2+}$ mechanism as being the dominant one. However as shown in **Figures 3A,B**, the use of EPMA totals to determine water contents in hydrous phases is unreliable. For example, analyses for ringwoodite samples 271 and sample 238 yield very different analysis totals of 97.6 and 100.4 wt%, respectively, implying rather different water contents. However, their similar (Mg+Fe)/Si ratios of 1.96 and 1.95 indicate similar water contents, as confirmed by ERDA with 0.43 and 0.44 wt% H_2O, respectively.

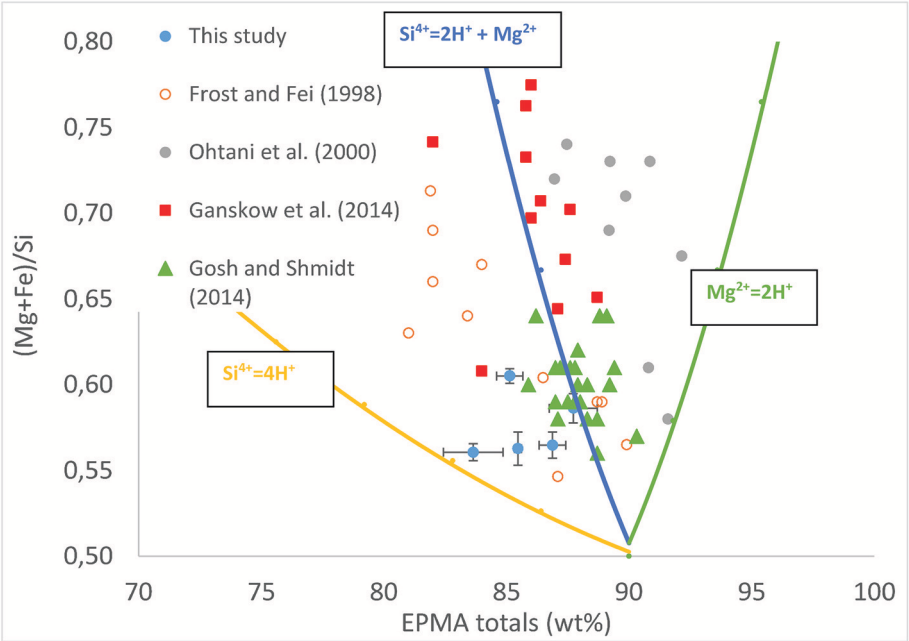

FIGURE 8 | Electron probe micro analyses showing the (Mg+Fe)/Si ratio in phase D as a function of analysis totals from this study compared to previous reports. Our results agree with those obtained at high temperatures by Frost and Fei (1998).

CONCLUSION

Hydrous wadsleyite and ringwoodite have been synthesized in the MgO-SiO_2-H_2O and MgO-FeO-SiO_2-H_2O systems at pressures from 15 to 22 GPa and temperatures from 1,100 to 1,700°C. Their water contents have been measured using Elastic Recoil Detection Analysis (ERDA) and vary from 0.02 to 3.1 wt% H_2O. For ringwoodite samples, containing up to 1.16 wt% H_2O, we observe that the (Mg+Fe)/Si ratio vs. water content follows the same trend as for wadsleyite, indicating that hydrogen is substituting for magnesium. Our measurements agree with the trends of (Mg+Fe)/Si vs. water observed for wadsleyite using SIMS but not for ringwoodite. At least at water contents below 1.2 wt% H_2O.

We also measured, for the first time, quantitative water contents of phase D and observed that it varies from 6.7 to 11.2 wt% H_2O (up to twice less than estimated from EPMA totals) and that the Mg/Si atomic ratio decreases with increasing water content, in disagreement with earlier data, but as we explained above our compositional field is very narrow compared to previous reports.

Using the samples from this study, we were able to determine the absorptivity coefficient for OH infrared absorption bands in four wadsleyite samples and five ringwoodite samples. The average for the two iron-free wadsleyite samples leads to an absorptivity of 69,000 ± 7,000 L/moles H_2O/cm^2, in very good agreement with that determined by Deon et al. (2010). The wadsleyite with 8 mole% Fe, displays an absorptivity of 67,000 ± 5,000 L/moles H_2O/cm^2. The absorptivity values vary from 118,000 ± 5,000 for ringwoodite without Fe to 135,000 ± 9,000 for Fe-bearing ringwoodite (10% mole Fe). Our values of ε for ringwoodite and wadsleyite agree well with those of Koch-Muller and Rhede (2010) and Deon et al. (2010). We thus confirm that the experimentally determined ε are lower than the trend reported in the calibration of Paterson (1982), but also lower than the trend reported in the calibration of Libowitzky and Rossman (1997) in the case of ringwoodite and wadsleyite. We find that the calibration of Paterson (1982) under-estimates the water contents by 50%. This should be taken into account when studying the effect of water on the elasticity of wadsleyite and ringwoodite.

AUTHOR CONTRIBUTIONS

NB-C is responsible for project design, funding, and wrote the manuscript. NB-C and DN are responsible for performing the multi-anvil experiments, ERDA, EPMA, and Raman measurements and data treatment. FS is responsible for the FTIR and Raman measurements on ringwoodite as well as assessing the extinction coefficients. HB, CR, and HK are responsible for the operation of the nuclear probe and standardization. SD brought two samples that were previously analyzed by SIMS.

ACKNOWLEDGMENTS

The authors thank G. Bromiley and S. Ghosh who reviewed and helped improve the manuscript. We thank Jean-Louis Fruquière for making the multi-anvil assembly parts, and Franck Pointud and Antoine Mathieu for maintenance and development of the

high-pressure lab. Jean-Luc Devidal and Jean-Marc Hénot are thanked for their help in EPMA and SEM analyses, respectively. We also acknowledge the LEEL's staff for their assistance during the nuclear microprobe analysis. This work was conducted in the framework of the ANR Jeune Chercheuse HYDEEP Hydrogen in the Deep Earth awarded to NB-C (ANR 11 JS56 01501). This work benefitted from Labex Clervolc grants to DN and FS. This is ClerVolc contribution n°303.

SUPPLEMENTARY MATERIAL

The Supplementary Material for this article can be found online at: https://www.frontiersin.org/articles/10.3389/feart.2018.00075/full#supplementary-material

Supplementary Figure 1 | Unpolarized spectra measured on different grains of four wadsleyite samples, which were used to calculate the average absorbance (Horiuchi and Sawamoto, 1981; Finger et al., 1993).

REFERENCES

Bali, E., Bolfan-Casanova, N., and Koga, K. T. (2008). Pressure and temperature dependence of H solubility in forsterite: an implication to water activity in the Earth interior. *Earth Planetar. Sci. Lett.* 268, 354–363. doi: 10.1016/j.epsl.2008.01.035

Bell, D. R., Ihingher, P. D., and Rossman, G. R. (1995). Quantitative analysis of trace OH in garnet and pyroxenes. *Am. Mineral.* 80, 465–474. doi: 10.2138/am-1995-5-607

Blanchard, M., Balan, E., and Wright, K. (2009). Incorporation of water in iron-free ringwoodite: a first-principles study. *Am. Mineral.* 94, 83–89. doi: 10.2138/am.2009.3020

Bolfan-Casanova, N., Keppler, H., and Rubie, D. C. (2000). Water partitioning between nominally anhydrous minerals in the MgO-SiO_2-H_2O system up to 24 GPa: implications for the distribution of water in the Earth's mantle. *Earth Planet. Sci. Lett.* 182, 209–221. doi: 10.1016/S0012-821X(00)00244-2

Bolfan-Casanova, N., Muñoz, M., McCammon, C., Deloule, E., Férot, A., Demouchy, S., et al. (2012). Ferric iron and water incorporation in wadsleyite under hydrous and oxidizing conditions: A XANES, Mossbauer, and SIMS study. *Am. Mineral.* 97, 1483–1493. doi: 10.2138/am.2012.3869

Boujibar, A., Denis, A., Mohamed, A. B., Bolfan-Casanova, N., and Jean-Luc, D., Nicolas, T., et al. (2014). Metal-silicate partitioning of sulphur, new experimental and thermodynamic constraints on planetary accretion. *Earth Planet. Sci. Lett.* 391, 42–54. doi: 10.1016/j.epsl.2014.01.021

Bureau, H., Raepsaet, C., Khodja, H., Carraro, A., and Aubaud, C. (2009). Determination of hydrogen content in geological *samples using elastic recoil detection analysis (ERDA). Geochim. Cosmochim. Acta* 73, 3311–3322. doi: 10.1016/j.gca.2009.03.009

Chang, Y.-Y., Jacobsen, S. D., Bina, C. R., Thomas, S. M., Smyth, J. R., Frost, D. J., et al. (2015). Comparative compressibility of hydrous wadsleyite and ringwoodite: effect of H2O and implications for detecting water in the transition zone. *J. Geophys. Res. Solid Earth* 120, 8259–8280. doi: 10.1002/2015JB012123

Daudin, L., Khodja, H., and Gallien, J. P. (2003). Development of "position-charge-time" tagged spectrometry for ion beam microanalysis. *Nucl. Instrum. Methods B* 210, 153–158. doi: 10.1016/S0168-583X(03)01008-5

Demouchy, S., and Bolfan-Casanova, N. (2016). Distribution and transport of hydrogen in the lithospheric mantle: a review. *Lithos* 240, 402–425. doi: 10.1016/j.lithos.2015.11.012

Demouchy, S., Deloule, E., Frost, D. J., and Keppler, H. (2005). Pressure and temperature-dependence of water solubility in Fe-free wadsleyite. *Am. Mineral.* 90, 1084–1091. doi: 10.2138/am.2005.1751

Deon, F., Koch-Müller, M., Rhede, D., Gottschalk, M., Wirth, R., and Thomas, S.-M. (2010). Location and quantification of hydroxyl in wadsleyite: new insights. *Am. Mineral.* 95, 312–322. doi: 10.2138/am.2010.3267

Finger, L. W., Hazen, R. M., Zhang, J. M., Ko, J. D., and Navrotsky, A. (1993). The effect of Fe on the crystal-structure of wadsleyite beta-(MG1-XFEX)2SIO4, 0.00-less-than-or-equal-to-x-less-than-or-equal-to-0.40. *Phys. Chem. Miner.* 19, 361–368. doi: 10.1007/BF00202973

Frost, D. (1999). "The stability of dense hydrous magnesium silicates in Earth's transition zone and lower mantle," in *Mantle Petrology: Field Observations and High Pressure Experimentation: A Tribute to F.R. Boyd*, eds Y. Fei, C. Bertka, and B. O. Mysen (Geochemical Society Special Publication), 283–296.

Frost, D. J., and Fei, Y. W. (1998). Stability of phase D at high pressure and high temperature. *J. Geophys. Res. Solid Earth* 103, 7463–7474. doi: 10.1029/98JB00077

Ganskow, G., Ballaran, T. B., and Langenhorst, F. (2010). Effect of iron on the compressibility of hydrous ringwoodite. *Am. Mineral.* 95, 747–753. doi: 10.2138/am.2010.3420

Ganskow, G., and Langenhorst, F. (2014). Stability and crystal chemistry of iron-bearing dense hydrous magnesium silicates. *Chemie Der Erde-Geochem.* 74, 489–496. doi: 10.1016/j.chemer.2014.06.001

Ghosh, S., and Schmidt, M. W. (2014). Melting of phase D in the lower mantle and implications for recycling and storage of H_2O in the deep mantle. *Geochim. Cosmoch. Acta* 145, 72–88. doi: 10.1016/j.gca.2014.06.025

Hazen, R. M., Zhang, J. M., and Ko, J. D. (1990). Effects of Fe/Mg on the compressibility of synthetic wadsleyite - beta-(Mg1-xfex)2SiO4(X less-than-or-equal-to 0.25). *Physics Chem. Min.* 17, 416–419.

Hofmeister, A. M., and Mao, H. K. (2001). Evaluation of shear moduli and other properties of silicates with the spinel structure from IR spectroscopy. *Am. Mineral.* 86, 622–639. doi: 10.2138/am-2001-5-604

Horiuchi, H., and Sawamoto, H. (1981). ß-Mg2SiO4: single-crystal X-ray study. *Am. Mineral.* 66, 568–575.

Huang, X., Xu, Y., and Karato, S. (2005). Water contetn in the transition zone from electrical conductivity of wadsleyite and ringwoodite. *Nature* 434, 746–749. doi: 10.1038/nature03426

Inoue, T. (1994). Effect of water on melting phase relations and melt composition in the system Mg2SiO4-MgSiO3-H2O up to 15 GPa. *Phys. Earth Planet. Inter.* 85, 237–263. doi: 10.1016/0031-9201(94)90116-3

Inoue, T., Weidner, D. J., Northrup, P. A., and Parise, J. B. (1998). Elastic properties of hydrous ringwoodite (?-phase) in Mg2SiO4. *Earth Planet. Sci. Lett.* 160, 107–113. doi: 10.1016/S0012-821X(98)00077-6

Inoue, T., Yurimoto, H., and Kudoh, Y. (1995). Hydrous modified spinel, Mg1.75SiH0.5O4: a new water reservoir in the mantle transition zone. *J. Geophys. Res.* 22, 117–120.

Jacobsen, S. D., Demouchy, S., Frost, D. J. B. B. T., and Kung, J. (2005). A systematic study of OH in hydrous wadsleyite from polarized infrared spectroscopy and single-crystal X- ray diffraction. *Am. Mineral.* 90, 61–70. doi: 10.2138/am.2005.1624

Kawamoto, T., Hervig, R. H., and Holloway, J. R. (1996). Experimental evidence for a hydrous transition zone in the early Earth's mantle. *Earth Planet. Sci. Lett.* 142, 587–592. doi: 10.1016/0012-821X(96)00113-6

Khodja, H., Berthoumieux, E., Daudin, L., and Gallien, J. P. (2001). The Pierre Süe Laboratory nuclear microprobe as a multidisciplinary analysis tool. *Nucl. Instrum. Methods B* 181, 83–86. doi: 10.1016/S0168-583X(01)00564-X

Koch-Muller, M., and Rhede, D. (2010). IR absorption coefficients for water in nominally anhydrous high-pressure minerals. *Am. Mineral.* 95, 770–775. doi: 10.2138/am.2010.3358

Kohn, S. C., Brooker, R. A., Frost, D. J., Slesinger, A. E., and Wood, B. J. (2002). Ordering of hydroxyl defects in hydrous wadsleyite (ß-Mg2SiO4). *Am. Mineral.* 87, 293–301. doi: 10.2138/am-2002-2-310

Kovacs, I., Hermann, J., O'Neill, H. C., Gerald, J. F., Sambridge, M., et al. (2008). Quantitative absorbance spectroscopy with unpolarized light: part II. *Experimental evaluation and development of a protocol for quantitative analysis of mineral IR spectra. Am. Mineral.* 93, 765–778. doi: 10.2138/am.2008.2656

Kröger, F. A., and Vink, H. H. (1956). Relations between the concentrations of imperfections in crystalline solids. *Solid State Physics* 3, 307–435. doi: 10.1016/S0081-1947(08)60135-6

Kudoh, Y., Inoue, T., and Arashi, H. (1996). Structure and crystal chemistry of hydrous wadsleyite, Mg1.75SiH0.5O4: possible hydrous magnesium silicate in the mantle transition zone. *Phys. Chem. Miner.* 23, 461–469.

Kudoh, Y., Kuribayashi, T., Mizobata, H., and Ohtani, E. (2000). Structure and cation disorder of hydrous ringwoodite, ?-Mg1.89Si0.98H0.30O4. *Phys. Chem. Miner.* 27, 474–479. doi: 10.1007/s002690000091

Libowitzky, E. (1999). Correlation of O-H stretching frequencies and O-H center dot center dot center dot O hydrogen bond lengths in minerals. *Monatshefte Fur Chemie* 130, 1047–1059.

Libowitzky, E., and Rossman, G. R. (1996). Principles of quantitative absorbance measurements in anisotropic crystals. *Phys. Chem. Miner.* 23, 319–327. doi: 10.1007/BF00199497

Libowitzky, E., and Rossman, G. R. (1997). An IR absorption calibration for water in minerals. *Am. Mineral.* 82, 1111–1115. doi: 10.2138/am-1997-11-1208

Mayer, M. (1999). "SIMNRA a simulation program for the analysis of NRA, RBS, and ERDA," in *Proceedings of the 15th International Conference on the Application of Accelerators in Research and Industry*, eds J. L. Duggan and I. L. Morgan (American Institute of Physics Conference Proceedings), 475, 541.

Mrosko, M., Lenz, S., McCammon, C. A., Taran, M., Wirth, R., and Koch-Müller, M. (2013). Hydrogen incorporation and the oxidation state of iron in ringwoodite: a spectroscopic study. *Am. Mineral.* 98, 629–636. doi: 10.2138/am.2013.4245

Novella, D., Frost, D. J., hauri, E. H., Bureau, H., Raepsaet, C., and Roberge, M. (2014). The distribution of H2O between silicate melt and nominally anhydrous peridotite and the onset of hydrous melting in the deep upper mantle. *Earth Planet. Sci. Lett.* 400, 1–13. doi: 10.1016/j.epsl.2014.05.006

Ohtani, E., Mizobata, H., Kudoh, Y., and Nagase, T. (1997). A new hydrous silicate, a water reservoir, in the upper part of the lower mantle. *Geophys. Res. Lett.* 24, 1047–1050. doi: 10.1029/97GL00874

Ohtani, E., Mizobata, H., and Yurimoto, H. (2000). Stability of dense hydrous magnesium silicate phases in the systems Mg2SiO4 -H2O and MgSiO3 -H2O at pressures up to 27 GPa. *Phys. Chem. Miner.* 27, 533–544. doi: 10.1007/s002690000097

Pamato, M. G., Myhill, R., Ballaran, T. B., Frost, D. J., Heidelbach, F., Miyajima, N. et al. (2015). Lower-mantle water reservoir implied by the extreme stability of a hydrous aluminosilicate. *Nat. Geosci.* 8, 75–79. doi: 10.1038/ngeo2306

Paterson, M. S. (1982). The determination of hydroxyl by infrared absorption in quartz, silicate glasses and similar materials. *Bull. Mineral.* 105, 20–29.

Pearson, D. G., Brenker, F. E., Nestola, F., McNeill, J., Nasdala, L., Hutchison, M. T., et al. (2014). Hydrous mantle transition zone indicated by ringwoodite included within diamond. *Nature* 507, 221–224. doi: 10.1038/nature13080

Purevjav, N., Okuchi, T., Tomioka, N., Abe, J., and Harjo, S. (2014). Hydrogen site analysis of hydrous ringwoodite in mantle transition zone by pulsed neutron diffraction. *Geophys. Res. Lett.* 41, 6718–6724. doi: 10.1002/2014GL061448

Raepsaet, C., Bureau, H., Khodja, H., Aubaud, C., and Carraro, A. (2008). μ-ERDA developments in order to improve the water content determination in hydrous and nominally anhydrous mantle phases. *Nucl. Instrum. Methods Phys. Res. B* 266, 1333–1337. doi: 10.1016/j.nimb.2008.01.028

Sambridge, M., Gerald, J. F., Kovacs, I., O'Neill, H. S. C., and Hermann, J. (2008). Quantitative absorbance spectroscopy with unpolarized light: Part I. *Physical and mathematical development. Am. Mineral.* 93, 751–764. doi: 10.2138/am.2008.2657

Sano-Furukawa, A., Kuribayashi, T., Komatsu, K., Yagi, T., and Ohtani, E. (2011). Investigation of hydrogen sites of wadsleyite: a neutron diffraction study. *Phys. Earth Planet. Interiors* 189, 56–62. doi: 10.1016/j.pepi.2011.07.003

Shieh, S. R., Mao, H. K., Hemley, R. J., and Ming, L. C. (1998). Decomposition of phase D in the lower mantle and the fate of dense hydrous silicates in subducting slabs. *Earth Planet. Sci. Lett.* 159, 13–23. doi: 10.1016/S0012-821X(98)00062-4

Smyth, J. R. (1994). A crystallographic model for hydrous wadsleyite (ß-Mg2SiO4): An ocean in the Earth's interior ? *Am. Mineral.* 79, 1021–1024.

Smyth, J. R., Bolfan-Casanova, N., Avignant, D., El-Ghozzi, M., and Hirner, S. M. (2014). Tetrahedral ferric iron in oxidized hydrous wadsleyite. *Am. Mineral.* 99, 458–466. doi: 10.2138/am.2014.4520

Smyth, J. R., Holl, C. M., Frost, D. J., Jacobsen, S. D., Langenhorst, F., and McCammon, C. A. (2003). Structural systematics of hydrous ringwoodite and water in Earth's interior. *Am. Mineral.* 88, 1402–1407. doi: 10.2138/am-2003-1001

Smyth, J. R., and Kawamoto, T. (1997). Wadsleyite II: a new high-pressure hydrous phase in the peridotite-H2O system. *Earth Planet. Sci. Lett.* 146, E9–E16. doi: 10.1016/S0012-821X(96)00230-0

Thomas, S. M., Jacobsen, S. D., Bina, C. R., Reichart, P., Moser, M., Hauri, E. H., et al., (2015). Quantification of water in hydrous ringwoodite. *Front. Earth Sci.* 2:38. doi: 10.3389/feart.2014.00038

Walter, M. J., Thomson, A. R., Wang, W., Lord, O. T., Ross, J., McMahon, S. C., et al. (2015). The stability of hydrous silicates in Earth's lower mantle: experimental constraints from the systems $MgO-SiO_2-H_2O$ and $MgO-Al_2O_3-SiO_2-H_2O$. *Chem. Geol.* 418, 16–29. doi: 10.1016/j.chemgeo.2015.05.001

Wang, Y. Q. (2004). Hydrogen standards in elastic recoil detection analysis. *Nucl. Instrum. Methods Phys. Res. B* 219–220, 115–124. doi: 10.1016/j.nimb.2004.01.038

Withers, A. C., Bureau, H., Raepsaet, C., and Hirschmann, M. M. (2012). Calibration of infrared spectroscopy by elastic recoil detection analysis of H in synthetic olivine. *Chem. Geol.* 334, 92–98. doi: 10.1016/j.chemgeo.2012.10.002

Yang, H. X., Prewitt, C. T., and Frost, D. J. (1997). Crystal structure of the dense hydrous magnesium silicate, phase D. *Am. Mineral.* 82, 651–654. doi: 10.2138/am-1997-5-627

Ye, Y., Brown, D. A., Smyth, J. R., Panero, W. R., Jacobsen, S. D., Chang, Y. Y., et al. (2012). Compressibility and thermal expansion of hydrous ringwoodite with 2.5(3) wt% H2O. *Am. Mineral.* 97, 573–582. doi: 10.2138/am.2012.4010

Yoshino, T., and Katsura, T. (2012). Re-evaluation of electrical conductivity of anhydrous and hydrous wadsleyite. *Earth Planet. Sci. Lett.* 337, 56–67. doi: 10.1016/j.epsl.2012.05.023

Conflict of Interest Statement: The authors declare that the research was conducted in the absence of any commercial or financial relationships that could be construed as a potential conflict of interest.

Copyright © 2018 Bolfan-Casanova, Schiavi, Novella, Bureau, Raepsaet, Khodja and Demouchy. This is an open-access article distributed under the terms of the Creative Commons Attribution License (CC BY). The use, distribution or reproduction in other forums is permitted, provided the original author(s) and the copyright owner are credited and that the original publication in this journal is cited, in accordance with accepted academic practice. No use, distribution or reproduction is permitted which does not comply with these terms.